Cyclopentadienylmolybdenum(II) and -(III) Complexes Containing Diene and Allyl Ligands. 3. Reactivity Studies of the Bis(butadiene) Complex [CpMo(s-cis-supine -η-C 4 H 6)(s-trans -η-C 4 H 6)][BF 4] †

Li-Sheng Wang, James Fettinger, Rinaldo Poli, Rita Meunier-Prest

Cyclopentadienylmolybdenum(II) and -(III) Complexes Containing Diene and Allyl Ligands. 3. Reactivity Studies of the Bis(butadiene) Complex [CpMo(*s-cis-supine-η*-C_4H_6)(*s-trans-η*-C_4H_6)][BF_4]†

Li-Sheng Wang,[1a] James C. Fettinger,[1a] Rinaldo Poli,*,[1b] and Rita Meunier-Prest[1b]

Laboratoire de Synthèse et d'Electrosynthèse Organométalliques, Faculté des Sciences "Gabriel", Université de Bourgogne, 6 Boulevard Gabriel, 21100 Dijon, France, and Department of Chemistry and Biochemistry, University of Maryland, College Park, Maryland 20742

Received December 9, 1997

The compound [CpMo(*s-cis-supine*-C_4H_6)(*s-trans*-C_4H_6)]BF_4 (**2**) reacts with a variety of nucleophilic reagents to afford either substitution of the *s-trans*-butadiene ligand or regioselective nucleophilic addition to the *endo* terminal carbon of the *s-trans* butadiene ligand. The reaction with ^{t}BuNC affords the substitution product [CpMo(*s-cis-supine*-C_4H_6)-(^{t}BuNC)$_2$]BF_4 (**3**). Nucleophilic addition of PMe_3 leads to [CpMo(*s-cis-supine*-C_4H_6)(*syn-prone*-C_3H_4-1-CH_2PMe_3)]BF_4 (**4**), which has been characterized also by X-ray crystallography. Nucleophilic addition of methyllithium or allylmagnesium bromide affords [CpMo(*s-cis-supine*-C_4H_6)(*syn-prone*-C_3H_4-1-CH_2R)]BF_4 (R = Me, (**5**), $CH_2CH{=}CH_2$ (**6**)). The Grignard reaction, however, also affords the substitution product CpMo(*s-cis-supine*-C_4H_6)(*prone*-C_3H_5). Compound **5** is oxidized by ferrocenium to [**5**]$^+$, which rapidly and extensively isomerizes to [CpMo(*s-cis-supine*-C_4H_6)(*syn-supine*-C_3H_4-1-Et)]$^+$ ([**7**]$^+$). Reduction of the latter by cobaltocene affords CpMo(*s-cis-supine*-C_4H_6)(*syn-supine*-C_3H_4-1-Et) (**7**), which isomerizes slowly ($t_{1/2}$ = 95 min at room temperature) to **5**. A cyclic voltammetric investigation of **5** and [**7**]$^+$ is consistent with the chemical redox experiments and yields kinetic and thermodynamic information on the interconversion between [**5**]$^+$ and [**7**]$^+$. Theoretical calculations rationalize the higher reactivity at the *s-trans* diene *endo* position for compound **2** as the result of a greater participation of the orbitals of this atom to the LUMO.

Introduction

In the course of our recent studies of cyclopentadienylmolybdenum(II) and -(III) complexes containing allyl and diene ligands,[2,3] we have established that the electron-rich isomeric complexes CpMo(η^3-C_3H_5)(η^4-C_4H_6) (**1a**−**c**; see Scheme 1) are not susceptible to nucleophilic attack, while the electrophilic attack by protons easily takes place. The position of attack and nature of the ultimate products depend on the coordination mode of the allyl and diene ligands in the starting compound and on the reaction conditions (especially the nature of the solvent) (see Scheme 1). It is particularly intriguing to observe that, in MeCN, the *s-trans* diene in **1c** is more susceptible to proton attack than the allyl ligand, whereas the allyl is always selectively attacked in **1a** or **1b**, where the diene ligand has the *s-cis* configuration. Calculations of charge distribution in **1a**−**c** by DFT methods have provided a rationalization of this difference, as well as details on the Mo−allyl and Mo−butadiene bonding as a function of the ligand conformation.[3]

Scheme 1

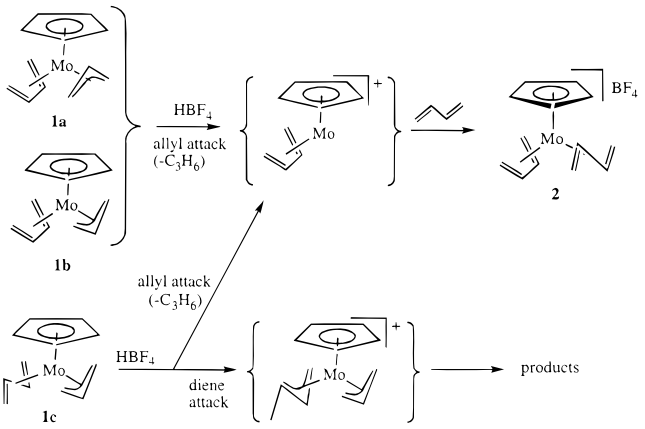

† Dedicated to Prof. Akira Nakamura on the occasion of his retirement.

(1) (a) University of Maryland. (b) Université de Bourgogne.

(2) Wang, L.-S.; Fettinger, J. C.; Poli, R. *J. Am. Chem. Soc.* **1997**, *119*, 4453−4464.

(3) Poli, R.; Wang, L.-S. *J. Am. Chem. Soc.* **1998**, *120*, 2831−2840.

The protonation of **1a** with HBF_4 in the presence of excess butadiene has led to the selective preparation of isomerically pure [CpMo(*s-cis-supine*-C_4H_6)(*s-trans*-C_4H_6)]BF_4 (**2**), isoelectronic with complexes **1**. There are few reported complexes containing a coordinated *s-trans* diene ligand,[4−12] and fewer still are those where both an *s-cis* and an *s-trans* diene are coordinated to the same metal center. The only such example known to us is CpNb(η^4-C_4H_6)$_2$, reported by Nakamura et al., but this is unfortunately obtained in admixture with the bis-*s-cis* isomer.[5]

We expected that the positive charge in **2**, relative to the precursor complexes **1**, would change the electronic properties of the coordinated diene ligand in favor of the reactivity toward nucleophiles. Nucleophilic additions to coordinated diene ligands have been extensively used in regiocontrolled organic synthetic applications, especially when the diene is functionalized by the $[CpMo(CO)_2]^+$ template.[13] However, this reaction has been mostly investigated for cyclic diene ligands. For acyclic dienes, studies have mostly been limited to the addition of nucleophiles such as hydride, vinylcuprates, and cyanide to *s-cis*-coordinated ligands.[13] There is only one reported study, to the best of our knowledge, of nucleophilic additions to a coordinated *s-trans* ligand, namely in the complexes $[CpMo(CO)_2(s\text{-}trans\text{-}CH_2{=}CH\text{-}CH{=}CHR)]^+$ (R = H, Me).[11] In many cases, studies of this nature are rendered difficult by the rapid transformation of the *s-trans* diene to the *s-cis* isomer.[8,11] The comparative reactivity of *s-cis* and *s-trans* diene ligands in the same coordination environment does not appear to have ever been investigated. Therefore, we have seen a unique opportunity to carry out such a study for complex **2**. The results of these investigations are the subject of the present contribution.

Experimental Section

General Procedures. All reactions were conducted by standard Schlenk-line techniques under a dinitrogen atmosphere. Solvents were dried by conventional methods (THF and Et_2O on Na/benzophenone, toluene and heptane on Na, CH_2Cl_2 on P_4O_{10}) and distilled directly from the drying agent under dinitrogen. All routine NMR experiments were carried out on Bruker AM400 and WF 200 spectrometers, while 2D NMR spectra were recorded on a Bruker AMX500 spectrometer. The ^1H and ^{13}C NMR data of all new compounds are given in Table 1. EPR spectra were recorded on a Bruker ER200 spectrometer and IR spectra on a Perkin-Elmer FTIR 1600 spectrophotometer. Cyclic voltammograms were recorded with a PRT 30 Tacussel potentiostat equipped with a home-built amplifier, a Hewlett-Packard 3314A function generator, and a Nicolet 450 digital oscilloscope or an X−Y Sefram plotter. The electrochemical cell was fitted with an SCE reference electrode and Pt working and counter electrodes. The supporting electrolyte used was 0.1 M $Bu^n_4NPF_6$. All potentials are reported vs the Cp_2Fe/Cp_2Fe^+ couple, which has an $E_{1/2}$ value of +0.50 V relative to SCE under conditions identical with those of the other experiments. Mass spectra were measured with a VG 7070E mass spectrometer. Elemental analyses were performed by Atlantic Microlab, Inc., or the analytical service at the LSEO, Dijon, France. [CpMo(*s-cis-supine*-η-C_4H_6)(*s-trans*-η-C_4H_6)][BF_4] (**2**) was prepared according to the literature procedure.[3]

Reactions of 2 with Bu^tNC. Formation of [CpMo($CNBu^t$)$_2$(*supine*-C_4H_6)][BF_4] (3). To a CD_3COCD_3 suspension of complex **2** (10 mg, 28 μmol in 0.5 mL) was added 2 equiv of *tert*-butyl isocyanide (6.3 μL, 56 μmol), followed by vigorous shaking. The suspension remained unchanged and no reaction was detected by ^1H NMR within 0.5 h. After it stood for 24 h at room temperature, most of the solid had dissolved and the ^1H NMR showed new resonances at δ 5.71 ($2H_a$, m), 5.33 (5H, Cp, s), 2.36 ($2H_b$, d, $^3J_{HH_a}$ = 7 Hz), 1.50 (18H, $CNBu^t$, s), and 1.20 ($2H_c$, d, $^3J_{HH_a}$ = 7.5 Hz), which are assigned to [CpMo($CNBu^t$)$_2$(*supine*-C_4H_6)][BF_4] (**3**) by comparison with the literature,[3] accompanied by the resonances at δ 6.35 (multiplet, 2H), 5.21 (doublet of multiplet, 2H), and 5.08 (doublet of multiplet, 2H) for free butadiene. Integration of the resonances shows the formation of **3** and C_4H_6 in a 1:1 ratio.

Reaction of 2 with PMe_3. Preparation of [CpMo(*syn*-Me_3PCH_2-*prone*-η-C_3H_4)(*s-cis-supine*-η-C_4H_6)][BF_4] (4). (i) NMR Monitoring. Compound **2** (10 mg, 0.028 mmol) was suspended in 0.5 mL of acetone-d_6 in an NMR tube. PMe_3 (5.8 μL, 0.056 mmol) was added by microsyringe, causing the formation of a yellow-brown solution. Monitoring by ^1H NMR spectroscopy showed the quantitative conversion of compound **2** to [CpMo(*syn*-Me_3PCH_2-*prone*-η-C_3H_5)(*s-cis-supine*-η-C_4H_6)][BF_4] (**4**), without the formation of significant amounts of other NMR-active byproducts.

(ii) Preparative Scale. To a suspension of compound **2** in acetone (200 mg, 0.56 mmol in 10 mL) was added PMe_3 (116 μL, 1.12 mmol). The suspension turned to a yellow-brown solution within 10 min. Stirring was continued for an additional 0.5 h at room temperature, yielding a green-yellow precipitate. The solution was filtered, the solvent was removed under reduced pressure, and the solid was washed with 5 mL of THF, giving a green-yellow solid (yield, 215 mg, 89%). $^{31}P\{^1H\}$ NMR: 18.9 ppm (doublet of doublets of doublets, $^2J_{H_gP}$ = 15 Hz, $^2J_{H_hP}$ = 15 Hz, $^3J_{H_fP}$ = 8 Hz). Anal. Calcd for $C_{16}H_{26}BF_4MoP$: C, 44.5; H, 6.1. Found: C, 44.2; H, 6.1. A single crystal for the X-ray analysis was obtained by vapor diffusion of diethyl ether into an acetone solution.

Reaction of 2 with MeLi. Preparation of CpMo(*syn*-Et-*prone*-η-C_3H_4)(*s-cis-supine*-η-C_4H_6) (5). (i) NMR Monitoring. To a suspension of complex **2** (5 mg, 0.014 mmol) in 0.5 mL of THF was added 10 μL of a MeLi solution (1.4 M in diethyl ether, 1 equiv) causing the dissolution of the yellow starting material and formation of an orange solution. All solvent was removed by rapid dinitrogen flow, followed by evaporation under reduced pressure for 5 min. C_6D_6 (0.5 mL) was subsequently added, and the solution was investigated by ^1H NMR. The entire operation took ca. 15 min from the mixing of the reagents. The NMR showed the formation of isomerically pure CpMo(*syn*-Et-*prone*-η-C_3H_4)(*s-cis-supine*-η-C_4H_6) (**5**).

(ii) Preparative Scale. To a suspension of complex **2** (200 mg, 0.562 mmol) in THF (20 mL) was added 1 equiv of MeLi (1.4 M in Et_2O, 0.4 mL, 0.56 mmol), resulting in the immediate formation of an orange solution. After 0.5 h of stirring at room

(4) Erker, G.; Kruger, C.; Muller, G. *Adv. Organomet. Chem.* **1985**, *24*, 1−39.
(5) Okamoto, T.; Yasuda, H.; Nakamura, A.; Kai, Y.; Kanehisa, N.; Kasai, N. *J. Am. Chem. Soc.* **1988**, *110*, 5008−5017.
(6) Christensen, N. J.; Hunter, A. D.; Legzdins, P. *Organometallics* **1989**, *8*, 930−940.
(7) Benyunes, S. A.; Day, J. P.; Green, M.; Al-Saadoon, A. W.; Waring, T. L. *Angew. Chem., Int. Ed. Engl.* **1990**, *29*, 1416−1417.
(8) Benyunes, S. A.; Binelli, A.; Green, M.; Grimshire, M. J. *J. Chem. Soc., Dalton Trans.* **1991**, 895−904.
(9) Christensen, N. J.; Legzdins, P.; Einstein, F. W. B.; Jones, R. H. *Organometallics* **1991**, *10*, 3070−3080.
(10) Christensen, N. J.; Legzdins, P.; Trotter, J.; Yee, V. C. *Organometallics* **1991**, *10*, 4021−4030.
(11) Vong, W.-J.; Peng, S.-M.; Lin, W.-J.; Liu, R.-S. *J. Am. Chem. Soc.* **1991**, *113*, 573−582.
(12) Carfagna, C.; Deeth, R. J.; Green, M.; Mahon, M. F.; McInnes, J. M.; Pellegrini, S.; Woolhouse, C. B. *J. Chem. Soc., Dalton Trans.* **1995**, 3975−3985.
(13) Pearson, A. J. In *Comprehensive Organometallic Chemistry II*; Wilkinson, G., Stone, F. G. A., Abel, E. W., Eds.; Pergamon: Oxford, U.K., 1995; Vol. 12, Part 6.3, pp 637−683.

Table 1. ^{1}H NMR Data for Compounds

compd	^{1}H NMR (δ)	^{13}C NMR (δ)
[CpMo(*syn*-Me_3PCH_2-*prone*-η-C_3H_5)(*s-cis-supine*-η-C_4H_6)][BF_4] (**4**)[a,b]	4.92 (5H, Cp, s), 4.58 (1H$_a$, ddd, $^3J_{HH_{a'}}$ = 8 Hz, $^3J_{HH_b}$ = 7 Hz, $^3J_{HH_c}$ = 9 Hz), 4.26 (1H$_{a'}$, ddd, $^3J_{HH_a}$ = 8 Hz, $^3J_{HH_{b'}}$ = 7 Hz, $^3J_{HH_{c'}}$ = 9 Hz), 2.91 (1H$_g$, ddd, $^2J_{HP}$ = 15 Hz, $^2J_{HH_b}$ = 12 Hz, $^3J_{HH_{f'}}$ = 3 Hz), 2.89 (1H$_b$, d, $^3J_{HH_a}$ = 7 Hz), 2.83 (1H$_d$, ddd, $^3J_{HH_e}$ = $^3J_{HH_f}$ = 10 Hz, $^3J_{HH_f}$′ = 9 Hz), 2.80 (1H$_{b'}$, d, $^3J_{HH_{a'}}$ = 7 Hz), 2.45 (1H$_h$, ddd, $^2J_{HP}$ = 15 Hz, $^2J_{HH_g}$ = 12 Hz, $^3J_{HH_{f'}}$ = 12 Hz), 1.94 (9H, $P(CH_3)_3$, d, $^2J_{HP}$ = 15 Hz), 1.49 (1H$_e$, dd, $^3J_{HH_d}$ = 10 Hz, $^2J_{HH_f}$ = 4 Hz), 1.18 (1H$_{f'}$, dddd, $^3J_{HH_d}$ = 9 Hz, $^3J_{HH_h}$ = 12 Hz, $^3J_{HH_g}$ = 3 Hz, $^3J_{HP}$ = 8 Hz), 0.87 (1H$_c$, dd, $^3J_{HH_a}$ = 9 Hz, $^2J_{HH_b}$ = 1.5 Hz), 0.73 (1H$_{c'}$, d, $^3J_{HH_{a'}}$ = 9 Hz), 0.55 (1H$_f$, dd, $^3J_{HH_d}$ = 10 Hz, $^3J_{HH_e}$ = 3.5 Hz)[a]	111.6 (1C$_a$, d, ^1J = 168 Hz), 107.7 (1C$_{a'}$, d, ^1J = 170 Hz), 91.5 (5C, Cp, dm, ^1J = 177 Hz), 71.4 (1C$_d$, d, ^1J = 156 Hz), 39.6 (1C$_{bc}$, t, ^1J = 156 Hz), 39.3 (1C$_{b'c'}$, t, ^1J = 156 Hz), 38.1 (1C$_{f'}$, dd, ^1J = 152 Hz, $^2J_{HP}$ = 12 Hz), 30.8 (1C$_{gh}$, dt, $^1J_{HP}$ = 40 Hz, ^1J = 132 Hz), 28.5 (1C$_{ef}$, t, ^1J = 154 Hz), 7.8 (3C, $P(CH_3)_3$, dq, $^1J_{HP}$ = 53 Hz, ^1J = 134 Hz)[b]
CpMo(*syn*-Et-*prone*-η-C_3H_4)(*s-cis-supine*-η-C_4H_6) (**5**)[c]	4.34 (1H$_{a'}$, ddd, $^3J_{HH_a}$ = $^3J_{HH_{b'}}$ = 7 Hz, $^3J_{HH_{c'}}$ = 9 Hz), 4.27 (5H, Cp, s), 3.99 (1H$_a$, ddd, $^3J_{HH_{a'}}$ = $^3J_{HH_b}$ = 7 Hz, $^3J_{HH_c}$ = 9 Hz), 2.86 (1H$_{b'}$, d, $^3J_{HH_{a'}}$ = 7 Hz), 2.76 (1H$_b$, d, $^3J_{HH_a}$ = 7 Hz), 2.34 (1H$_d$, ddd, $^3J_{HH_e}$ = $^3J_{HH_f}$ = $^3J_{HH_{f'}}$ = 10 Hz), 1.68 (1H$_g$, m), 1.49 (1H$_e$, $^3J_{HH_d}$ = 9 Hz, $^2J_{HH_f}$ = 3 Hz), 1.44 (1H$_h$, m), 1.33 (1H$_{f'}$, ddd, $^3J_{HH_d}$ = 10 Hz, $^3J_{HH_g}$ = $^3J_{HH_h}$ = 7 Hz), 1.08 (3H$_i$, dd, $^3J_{HH_g}$ = $^3J_{HH_h}$ = 7 Hz), 0.63 (1H$_{c'}$, d, $^3J_{HH_{a'}}$ = 9 Hz), 0.51 (1H$_f$, m), 0.49 (1H$_c$, m)	110.3 (1C$_{a'}$, d, ^1J = 164 Hz), 106.2 (1C$_a$, d, ^1J = 163 Hz), 89.5 (5C, Cp, dm, ^1J = 177 Hz), 72.0 (1C$_d$, d, ^1J = 158 Hz), 58.3 (1C$_{f'}$, d, ^1J = 147 Hz), 39.8 (1C$_{b'c'}$, t, ^1J = 156 Hz), 38.2 (1C$_{bc}$, t, ^1J = 156 Hz), 30.0 (1C$_{hg}$, t, ^1J = 124 Hz), 28.2 (1C$_{ef}$, t, ^1J = 152 Hz), 18.6 (3C$_i$, ^1J = 126 Hz)
CpMo(*syn*-CH_2=$CH(CH_2)_2$-*prone*-η-C_3H_4)(*s-cis-supine*-η-C_4H_6) (**6**)[c]	5.91 (1H$_j$, ddt, $^3J_{HH_k}$ = 17.5 Hz, $^3J_{HH_l}$ = 10 Hz, $^3J_{HH_i}$ = 6.5 Hz), 5.11 (1H$_k$, ddt, $^3J_{HH_j}$ = 17.5 Hz, $^2J_{HH_l}$ = 2 Hz, $^4J_{HH_i}$ = 2 Hz), 5.05 (1H$_l$, ddt, $^3J_{HH_j}$ = 10 Hz, $^2J_{HH_k}$ = 2 Hz, $^4J_{HH_i}$ = 2 Hz), 4.35 (1H$_{a'}$, ddd, $^3J_{HH_a}$ = $^3J_{HH_{b'}}$ = 7 Hz, $^3J_{HH_{c'}}$ = 8.5 Hz), 4.25 (5H, Cp, s), 3.99 (1H$_a$, ddd, $^3J_{HH_{a'}}$ = $^3J_{HH_b}$ = 7 Hz, $^3J_{HH_c}$ = 8.5 Hz), 2.81 (1H$_{b'}$, $^3J_{HH_{a'}}$ = 7 Hz), 2.76 (1H$_b$, $^3J_{HH_a}$ = 7 Hz), 2.33 (1H$_d$, ddd, $^3J_{HH_e}$ = $^3J_{HH_f}$ = $^3J_{HH_{f'}}$ = 10 Hz), 2.20 (2H$_i$, ddd, $^3J_{HH_j}$ = 6.5 Hz, $^3J_{HH_g}$ = $^3J_{HH_h}$ = 7 Hz), 1.62 (1H$_g$ and 1H$_h$, m), 1.47 (1H$_e$, $^3J_{HH_d}$ = 9 Hz, $^2J_{HH_f}$ = 3.5 Hz), 1.34 (1H$_{f'}$, ddd, $^3J_{HH_d}$ = 10 Hz, $^3J_{HH_g}$ = 8 Hz, $^3J_{HH_h}$ = 6.5 Hz), 0.61 (1H$_{c'}$, d, $^3J_{HH_{a'}}$ = 9 Hz), 0.50 (1H$_f$, m), 0.49 (1H$_c$, m)	139.5 (1C$_j$, d, ^1J = 156 Hz), 114.4 (1C$_{kl}$, t, ^1J = 156 Hz), 110.2 (1C$_{a'}$, d, ^1J = 162 Hz), 106.4 (1C$_a$, d, ^1J = 162 Hz), 89.5 (5C, Cp, dm, ^1J = 177 Hz), 72.3 (1C$_d$, d, ^1J = 153 Hz), 54.9 (1C$_{f'}$, d, ^1J = 150 Hz), 39.7 (1C$_{b'c'}$, t, ^1J = 148 Hz), 38.6 (1C$_i$, t, ^1J = 128 Hz), 38.3 (1C$_{bc}$, t, ^1J = 148 Hz), 36.5 (1C$_{hg}$, t, ^1J = 124 Hz), 28.2 (1C$_{ef}$, t, ^1J = 153 Hz)
CpMo(*syn*-Et-*supine*-η-C_3H_4)(*s-cis-supine*-η-C_4H_6) (**7**)[a]	4.49 (1H$_{a'}$, ddd, $^3J_{HH_a}$ = $^3J_{HH_{b'}}$ = 7 Hz, $^3J_{HH_{c'}}$ = 9.5 Hz), 4.39 (5H, Cp, s), 4.29 (1H$_a$, ddd, $^3J_{HH_{a'}}$ = $^3J_{HH_b}$ = 7 Hz, $^3J_{HH_c}$ = 9 Hz), 3.97 (1H$_d$, ddd, $^3J_{HH_e}$ = 7 Hz, $^3J_{HH_f}$ = $^3J_{HH_{f'}}$ = 12 Hz), 2.51 (1H$_{b'}$, d, $^3J_{HH_{a'}}$ = 7 Hz), 2.45 (1H$_e$, $^3J_{HH_d}$ = 7 Hz), 2.1 (1H$_b$, overlapping with the solvent signal), 1.95 (1H$_h$, m), 1.75 (1H$_g$, m), 1.02 (3H$_i$, dd, $^3J_{HH_g}$ = $^3J_{HH_h}$ = 7.5 Hz), 1.0 (1H$_f$ and 1H$_{f'}$, overlapping with H$_i$), 0.50 (1H$_{c'}$, d, $^3J_{HH_{a'}}$ = 9.5 Hz), 0.26 (1H$_c$, d, $^3J_{HH_a}$ = 9 Hz)	

[a] Acetone-d_6. [b] Acetonitrile-d_3. [c] C_6D_6.

temperature, all solvent was removed under reduced pressure. The product was extracted with 2 × 20 mL of heptane, followed by filtration and solvent removal under reduced pressure, to yield an yellow oil (yield 310 mg). Low-resolution mass spectrum (FAB+): *m/z* 286 [CpMo(Et-C_3H_4)(C_4H_6)]$^+$, 38%. The experimental isotopic envelope is in excellent agreement with the simulation. Cyclic voltammetry (THF, room temperature): ECE process with electrochemical oxidation for **5** at $E_{1/2}$ = −0.50 V (ΔE_p = 60 mV), followed by chemical transformation to **7**/**7**$^+$ (see Results).

Reaction of 5 with HBF_4. Formation of *trans*-2-Pentene. Complex **5** (5 mg, 17.6 μmol) was dissolved in 0.5 mL of C_6D_6. HBF_4·Et_2O (3 μL) was added by microsyringe, causing the precipitation of a gray solid. ^{1}H and ^{13}C NMR showed the formation of *trans*-2-pentene. ^{1}H NMR (C_6D_6, δ): 5.39 (m, 2H), 1.93 (m, 2H), 1.58 (d, 3H), 0.91 (t, 3H). ^{13}C{^{1}H} NMR (C_6D_6, δ): 133.3 (1C), 123 (1C), 25.9 (1C), 18.0 (1C), 12.4 (1C).

Reaction of 2 with C_3H_5MgBr. Formation of CpMo(*syn*-CH_2=$CHCH_2CH_2$-*prone*-η-C_3H_4)(*s-cis-supine*-η-C_4H_6) (6). To a suspension of complex **2** (400 mg, 1.12 mmol) in THF (20 mL) was added allylmagnesium bromide (1 M in Et_2O, 1.1 mL, 1.1 mmol) by syringe, causing the immediate formation of a yellow-brown solution. The solution was stirred overnight, followed by solvent removal under reduced pressure. The product was extracted with heptane (40 + 20 mL), followed by filtration. Evaporation of the solvent under reduced pressure gave an oily residue. Investigation of this residue by ^{1}H NMR showed the formation of the new complex CpMo(*syn*-CH_2=$CHCH_2CH_2$-*prone*-η-C_3H_4)(*s-cis-supine*-η-C_4H_6) (**6**) and CpMo(*prone*-η-C_3H_5)(*s-cis-supine*-η-C_4H_6) (**1a**). The latter was recognized by comparison of its NMR properties with those reported previously.[2] Integration of the ^{1}H NMR resonance gave a **6**/**1a** ratio of 90:10. Low-resolution mass spectrum (FAB+): *m/z* 312 [CpMo(CH_2=$CHCH_2CH_2C_3H_4$)(C_4H_6)]$^+$, 17%. The experimental isotopic envelope is in excellent agreement with the simulation.

Oxidation of 5 by $FcPF_6$. Preparation of [CpMo(*syn*-Et-*supine*-η-C_3H_4)(*s-cis-supine*-η-C_4H_6)][PF_6] ([7]PF_6). (i) Preparative Scale. A solution of compound **5** in heptane (190 mg, 0.669 mmol in 1 mL) was added to a solution of ferrocenium hexafluorophosphate (221 mg, 0.668 mmol) in acetone (30 mL). The purple-violet solution initially turned green and then changed to dark brown within seconds. After filtration, the volume of the solution was reduced to 5 mL under reduced pressure. Upon addition of 20 mL of THF, black needle-shaped crystals formed. The mother liquor was filtered off, and the solid was washed with 5 mL of THF and dried under vacuum for 1 h (yield 100 mg, 35%). Anal. Calcd for $C_{14}H_{20}MoPF_6$: C, 39.2; H, 4.7. Found: C, 38.4; H, 4.6. EPR (acetone): g = 2.029 (sextet with Mo satellites, a_H = 7 G; a_{Mo} = 33 G). Cyclic voltammetry (THF, room temperature): reversible reduction at $E_{1/2}$ = −0.86 V.

(ii) Spectroscopic EPR Monitoring. An EPR tube was charged with complex **5** (1 mg, 3 μmol) and Cp_2FePF_6 (1 mg, 3 μmol). Acetone (200 μL) was added at −196 °C. The mixture was thawed to −80 °C only immediately before the introduction into the EPR probe. The reaction was monitored by EPR, with gradual elevation of the temperature from −80 to 25 °C in increments of 20 °C. At −80 °C, the green mixture showed a major EPR signal at $g = 2.039$ ($a_{4H} = 8$ G, $a_{Mo} = 28$ G), which was assigned to $[\mathbf{5}]^+$, and a minor signal at $g = 2.034$. The intensity of the two species remained unchanged 20 min. As the temperature was increased to −20 °C, the original major species disappeared over 20 min, while the original minor species gained intensity. At 25 °C this species showed a signal at $g = 2.029$ ($a_{5H} = 7$ G, $a_{Mo} = 33$ G), corresponding to $[\mathbf{7}]^+$ (see previous section).

Reduction of $[7]PF_6$ by Cp_2Co. Formation of CpMo(*syn*-Et-*supine*-η-C_3H_4)(*s-cis-supine*-η-C_4H_6) (7). $[\mathbf{7}]PF_6$ (5 mg, 7.8 μmol) and Cp_2Co (1.5 mg) were placed in an NMR tube, to which 0.5 mL of acetone-d_6 was subsequently added. An instant reaction took place with the formation of a violet solution and precipitate. Monitoring by ^1H NMR revealed the selective formation of complex **7**, followed by its slow conversion to **5** with the half-life $t_{1/2} = 95$ min.

X-ray Crystallography for Compound 4. A yellow crystal with dimensions 0.500 × 0.213 × 0.100 mm was placed and optically centered on the Enraf-Nonius CAD-4 diffractometer. The cell parameters and crystal orientation matrix were determined from 25 reflections in the range $17.7 < \theta < 19.58°$ and confirmed with axial photographs. Data collection (3783 reflections in the $-h,k,l$ and $-h,k,-l$ and $h,-k,-l$ octants) and reduction were routine. A decay correction was not necessary, whereas an absorption correction based upon crystal faces was applied (T in the 0.8442−0.9229 range). Averaging of equivalent data gave 3311 unique intensities (R(int) = 0.0206). Systematic absences from the data uniquely determined the space group as $P2_12_12_1$ (No. 19). Direct methods resulted in the successful location of the Mo and P atoms and several C atoms. The remaining non-hydrogen atoms were located from two subsequent difference Fourier maps, alternating with full-matrix least-squares refinement cycles. Hydrogen atoms attached to carbon atoms were placed in calculated positions and continually updated but not refined. All of the non-hydrogen atoms were refined anisotropically. As the refinement converged, the absolute structure parameter, Flack(x), was refined to 0.40. The structure was inverted with the Flack(x) parameter refined to 0.37. At this point, a racemic twinning model was used, leading to refinement of the BASF parameter, equivalent to the Flack(x) parameter, at a value of 0.52(6). This indicates that the correct structure is composed of both enantiomorphs. The structure was refined to convergence ($\Delta/\sigma \leq 0.001$) with $R(F) = 5.03$, $R_w(F^2) = 7.83\%$, and GOF = 1.055 for all 3311 unique reflections [$R(F) = 3.41\%$, $R_w(F^2) = 7.13\%$ for those 2749 data with $F_o > 4\sigma(F_o)$]. A final difference Fourier map was featureless with $|\Delta\rho| \leq 0.43$ e Å^{-3}, indicating that the structure is both correct and complete. Relevant crystal and refinement parameters are collected in Table 2, and selected bond distances and angles are given in Table 3.

Theoretical Calculations. The geometry of the [CpMo(*s-cis-supine*-C_4H_6)(*s-trans*-C_4H_6)]$^+$ cation was optimized at the DFT-B3LYP level.[14] The calculations were run using GAUSSIAN 94[15] on the SGI Power Challenge at the Université de Bourgogne. The LanL2DZ basis set used includes both Dunning and Hayís D95 sets for H and C[16] and the relativistic electron core potential (ECP) sets of Hay and Wadt for the Mo atom.[17−19] Electrons outside the core were all those of H and C atoms and the 4s, 4p, 4d, and 5s electrons for Mo. Molecular orbital calculations were also carried out by the Fenske−Hall method[20] on the B3LYP-optimized geometry, using version 5.1 of the program for the Macintosh.[21] The default basis functions used by the program are generated by the numerical Xα atomic orbital program of Herman and

Table 2. Relevant Crystal Refinement Data for Compound 4

empirical formula	$C_{16}H_{26}BF_4MoP$
fw	432.09
temp	153(2) K
wavelength	0.710 73 Å
cryst system	orthorhombic
space group	$P2_12_12_1$
unit cell dimens	$a = 7.6932(4)$ Å
	$b = 12.5350(9)$ Å
	$c = 19.455(2)$ Å
	$\alpha = 90°$
	$\beta = 90°$
	$\gamma = 90°$
V, Z	1876.1(3) Å^3, 4
density (calcd)	1.530 Mg/m^3
abs coeff	0.815 mm^{-1}
F(000)	880
cryst size	0.500 × 0.2125 × 0.100 mm
θ range for data collectn	1.93−25.03°
no. of collected, indep rflns	3783, 3311 (R(int) = 0.0206)
max and min transmissn	0.9229 and 0.8442
no. of data/restraints/params	3311/0/212
goodness of fit on F^2	1.055
final R indices ($I > 2\sigma(I)$)[a]	R1 = 0.0341, wR2 = 0.0713 (2749 data)
R indices (all data)[a]	R1 = 0.0503, wR2 = 0.0783
largest diff peak and hole	0.425 and −0.344 e Å^{-3}

[a] $wR2 = \sum w(F_o^2 - F_c^2)$; $w = 1/[\sigma^2(F_o^2) + (0.0487P)^2 + 0.2288P]$; $P = (\max(F_o^2,0) + 2F_c^2)/3$.

Table 3. Selected Bond Distances (Å) and Angles (deg) for Compound 4

Mo(1)−C(1)	2.284(5)	Mo(1)−C(12)	2.283(5)
Mo(1)−C(2)	2.289(4)	C(1)−C(2)	1.383(7)
Mo(1)−C(3)	2.310(5)	C(1)−C(5)	1.398(7)
Mo(1)−C(4)	2.367(5)	C(2)−C(3)	1.410(7)
Mo(1)−C(5)	2.338(5)	C(3)−C(4)	1.400(8)
Mo(1)−CNT[a]	1.991(5)	C(4)−C(5)	1.385(7)
Mo(1)−C(6)	2.251(5)	C(6)−C(7)	1.403(8)
Mo(1)−C(7)	2.336(5)	C(7)−C(8)	1.377(8)
Mo(1)−C(8)	2.341(5)	C(8)−C(9)	1.401(7)
Mo(1)−C(9)	2.240(5)	C(10)−C(11)	1.423(6)
Mo(1)−C(10)	2.280(4)	C(11)−C(12)	1.408(8)
Mo(1)−C(11)	2.210(4)	C(12)−C(13)	1.511(6)
CNT−Mo−C(6)[a]	108.2(2)	CNT−Mo−C(11)[a]	111.5(2)
CNT−Mo−C(7)[a]	141.9(2)	CNT−Mo−C(12)[a]	122.5(2)
CNT−Mo−X(67)[a]	125.6(2)	CNT−Mo−X(1011)[a,b]	117.6(2)
CNT−Mo−C(8)[a]	140.3(2)	CNT−Mo−X(1112)[a,b]	118.5(2)
CNT−Mo−C(9)[a]	106.0(2)	C(6)−C(7)−C(8)	121.3(6)
CNT−Mo−X(89)[a]	123.7(2)	C(7)−C(8)−C(9)	120.6(6)
CNT−Mo−C(10)[a]	120.7(2)	C(10)−C(11)−C(12)	122.4(7)

[a] CNT = centroid of C(1) through C(5) atoms. [b] X(nm) = centroid of atoms C(m) and C(n).

(14) Becke, A. D. *J. Chem. Phys.* **1993**, *98*, 5648.

(15) Frisch, M. J.; Trucks, G. W.; Schlegel, H. B.; Gill, P. M. W.; Johnson, B. G.; Robb, M. A.; Cheeseman, J. R.; Keith, T. A.; Petersson, G. A.; Montgomery, J. A.; Raghavachari, K.; Al-Laham, M. A.; Zakrzewski, V. G.; Ortiz, J. V.; Foresman, J. B.; Cioslowski, J.; Stefanov, B. B.; Nanayakkara, A.; Challacombe, M.; Peng, C. Y.; Ayala, P. Y.; Chen, W.; Wong, M. W.; Andres, J. L.; Replogle, E. S.; Gomperts, R.; Martin, R. L.; Fox, D. J.; Binkley, J. S.; Defrees, D. J.; Baker, J.; Stewart, J. P.; Head-Gordon, M.; Gonzales, C.; Pople, J. A. Gaussian 94 (Revision E.1); Gaussian, Inc.: Pittsburgh, PA, 1995.

(16) Dunning, T. H., Jr.; Hay, P. J. In *Modern Theoretical Chemistry*; Schaefer, H. F., III, Ed.; Plenum Press: New York, 1976; pp 1−28.

(17) Hay, P. J.; Wadt, W. R. *J. Chem. Phys.* **1985**, *82*, 270−283.

(18) Hay, P. J.; Wadt, W. R. *J. Chem. Phys.* **1985**, *82*, 299−310.

(19) Wadt, W. R.; Hay, P. J. *J. Chem. Phys.* **1985**, *82*, 284−298.

(20) Hall, M. B.; Fenske, R. F. *Inorg. Chem.* **1972**, *11*, 768.

(21) Hall, M. B. Fenske−Hall Molecular Orbital Program; Texas A&M University, College Station, TX, 1989.

Skillman[22] used in conjunction with the Xα-to-Slater basis program of Bursten and Fenske.[23,24]

Results

Addition of Nucleophilic Reagents to Compound 2. The bis(butadiene) complex [CpMo(*s-cis-supine-η*-C_4H_6)(*s-trans-η*-C_4H_6)][BF_4] (**2**) readily reacts with a variety of nucleophilic reagents, i.e., MeCN, ^{t}BuNC, PMe_3, and Grignard reagents. The reaction path followed, however, differs depending on the reagent chosen. We have already reported that dissolution of compound **2** in MeCN leads to the substitution of the *s-trans* butadiene ligand with two molecules of the solvent.[3] An analogous exchange process occurs upon treatment of **2** with 2 equiv of *tert*-butyl isocyanide, to quantitatively yield the substitution product [CpMo(*supine*-C_4H_6)($CNBu^t$)$_2$][BF_4] (**3**) and 1 equiv of butadiene (see eq 1). Compound **3** was previously obtained

$$[\mathrm{CpMo}(s\text{-}cis\text{-}supine\text{-}\eta\text{-}C_4H_6)(s\text{-}trans\text{-}\eta\text{-}C_4H_6)]^+ + 2\mathrm{L} \rightarrow [\mathrm{CpMo}(s\text{-}cis\text{-}supine\text{-}\eta\text{-}C_4H_6)\mathrm{L}_2]^+ + C_4H_6 \quad (1)$$

$$\mathrm{L} = \mathrm{MeCN},\ ^t\mathrm{BuNC}$$

from the addition of ^{t}BuNC to [CpMo(*supine*-C_4H_6)(η^2-μ-F_2BF_2)]$_x$. These substitution reactions are indicative of the greater lability of the *s-trans* butadiene ligand.

Reaction of **2** with PMe_3 leads instead to the selective nucleophilic attack at the endo terminal position of the *s-trans* butadiene ligand to form a substituted allyl ligand (see eq 2). Due to the low symmetry of the

$$[\mathrm{CpMo}(s\text{-}cis\text{-}supine\text{-}\eta\text{-}C_4H_6)(s\text{-}trans\text{-}\eta\text{-}C_4H_6)]^+ + \mathrm{PMe}_3 \rightarrow [\mathrm{CpMo}(syn\text{-}prone\text{-}\eta\text{-}C_3H_4\text{-}1\text{-}CH_2PMe_3)(s\text{-}cis\text{-}supine\text{-}\eta\text{-}C_4H_6)]^+ \quad (2)$$

product [CpMo(*syn-prone-η*-C_3H_4-1-CH_2PMe_3)(*s-cis-supine-η*-C_4H_6)][BF_4] (**4**), all butadiene and allyl protons have different chemical shifts. The complete assignment of the ^{1}H NMR spectrum (Table 1) was assisted by a ^{1}H homonuclear selective decoupling experiment (see **I** for the proton nomenclature).

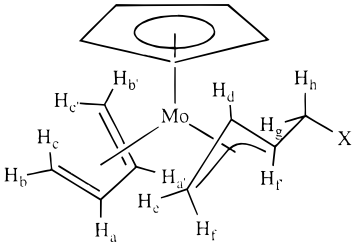

(X = -PMe_3^+, -CH_3, -CH_2-CH=CH_2)

I

The determination of the conformation of the butadiene and allyl ligands is based on the chemical shifts and geminal coupling constants of corresponding protons, following the same analysis described in detail earlier for compound **1c**.[2] The diastereotopic protons H_g and H_h of the methylene group resonate at δ 2.91 and 2.45, both as doublets of doublets of doublets because of geminal coupling with each other, with the adjacent allyl proton, and with the phosphorus nucleus. While the phosphorus couplings are identical (15 Hz), the coupling constants with $H_{f'}$ are quite different (3 Hz vs 12 Hz), reflecting a preferential conformation of the CH_2PMe_3 group with substantially distinct $H_{f'}CCH_g$ and $H_{f'}CCH_h$ dihedral angles. The phosphorus nucleus also exhibits an observable (8 Hz) three-bond coupling to the allyl anti proton $H_{f'}$, which is evidenced both in the ^{1}H and in the ^{31}P NMR spectrum. The structure of compound **4** is further confirmed by a single-crystal X-ray analysis (vide infra).

Treatment of **2** with 1 equiv of methyllithium immediately yields a yellow-brown solution of CpMo(*syn*-Et-*prone-η*-C_3H_4)(*s-cis-supine-η*-C_4H_6) (**5**) (see eq 3). No

$$[\mathrm{CpMo}(s\text{-}cis\text{-}supine\text{-}\eta\text{-}C_4H_6)(s\text{-}trans\text{-}\eta\text{-}C_4H_6)]^+ + \mathrm{R}^- \rightarrow \mathrm{CpMo}(syn\text{-}\mathrm{RCH}_2\text{-}prone\text{-}\eta\text{-}C_3H_4)(s\text{-}cis\text{-}supine\text{-}\eta\text{-}C_4H_6) \quad (3)$$

R = Me from MeLi or $CH_2CH{=}CH_2$ from C_3H_5MgBr

trace of compound **7** (vide infra) is observed in this reaction. As shown in Table 1, the spectroscopic properties of **5** are similar to those of compound **4**; thus, an identical structure (i.e. **I**) is proposed. Again, all allyl and diene hydrogen atoms are chemically inequivalent because of the low symmetry. The diastereotopic methylene protons (located at 1.68 and 1.44 ppm) show in this case identical coupling with proton $H_{f'}$. The relative upfield shift of these protons, as well as of the Cp, butadiene, and allyl protons, relative to those of complex **4** can be rationalized by the inductive effect of the methyl vs the phosphonium group. A positive NOE effect between H_a and H_f and between $H_{a'}$ and $H_{f'}$ can be taken as further evidence that the ethyl group occupies a syn position. A positive NOE effect was also observed between H_a and H_f in the symmetric compound CpMo(*prone-η*-C_3H_5)(*s-cis-supine-η*-C_4H_6) (**1a**).[2]

Treatment of **2** with allylmagnesium bromide yields a mixture of CpMo(*syn*-$CH_2{=}CH(CH_2)_2$-*prone-η*-C_3H_4)(*s-cis-supine-η*-C_4H_6) (**6**) and CpMo(*prone-η*-C_3H_5)(*s-cis-supine-η*-C_4H_6) (**1a**) in a 90:10 ratio. The two products may be rationalized by a competition of the two established reaction pathways: 90% of nucleophilic attack at the *s-trans* diene terminal carbon according to eq 3, and 10% of substitution of the *s-trans* diene ligand according to eq 1. The diastereotopic methylene protons in compound **6** overlap at ca. 1.62 ppm. The proton signals of the terminal vinyl group ($-CH_j{=}CH_kH_l$) are found in the typical range, indicating that this group is not coordinated to the metal center. The chemical shifts of other protons of **6** are close to the same protons of **5**, indicating that similar geometries and conformations are adopted by both complexes.

X-ray Structure of Compound 4. The nature of the PMe_3 addition product as the proposed [CpMo(*syn-prone-η*-C_3H_4-1-CH_2PMe_3)(*s-cis-supine-η*-C_4H_6)][BF_4] has been confirmed by an X-ray structural study. A view of the cation is shown in Figure 1. The overall geometry, conformation of the allyl and diene ligands, and

(22) Herman, F.; Skillman, S. *Atomic Structure Calculations*; Prentice Hall: Englewood Cliffs, NJ, 1963.
(23) Bursten, B. E.; Fenske, R. F. *J. Chem. Phys.* **1977**, *67*, 3138.
(24) Bursten, B. E.; Jensen, R. J.; Fenske, R. F. *J. Chem. Phys.* **1978**, *68*, 3320.

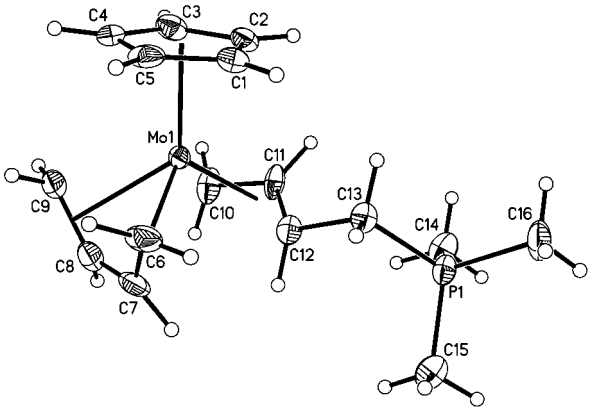

Figure 1. View of the cation in compound **4** with the numbering scheme employed. Ellipsoids are drawn at the 30% probability level.

metal−ligand bond lengths are quite comparable with those of the parent complex CpMo(*prone*-η-C_3H_4)(*s-cis-supine*-η-C_4H_6) (**1a**).[2] For the butadiene ligand, the lateral Mo−C bonds are shorter than the internal ones (average $\Delta d = -0.093$ Å; cf. -0.065 Å for **1a**) and the lateral C−C bonds are longer than the central one by 0.025 Å (cf. 0.032 Å for **1a**). The allyl ligand has longer lateral Mo−C bonds (by 0.072 Å, cf. 0.086 Å for **1a**).

Chemical and Electrochemical Oxidation of Compound 5. The low-temperature oxidation of CpMo(*syn-prone*-η-C_3H_4-1-Et)(*s-cis-supine*-η-C_4H_6) (**5**) by ferrocenium hexafluorophosphate in acetone initially gives the unstable green intermediate [CpMo(*syn-prone*-η-C_3H_4-1-Et)(*s-cis-supine*-η-C_4H_6)][PF_6] ([**5**]$^+PF_6^-$). However, this transforms rapidly to the violet isomer [CpMo(*syn-supine*-η-C_3H_4-1-Et)(*s-cis-supine*-η-C_4H_6)]-[PF_6] ([**7**]$^+PF_6^-$) upon warming to room temperature. This behavior is identical with that of the previously reported parent complex **1a**, where oxidation to green [**1a**]$^+$ is followed by a rapid isomerization to violet [**1b**]$^+$.[2]

The EPR spectrum of green [**5**]$^+$ can only be observed by carrying out the oxidation reaction directly in the EPR tube at −80 °C, although extensive isomerization to the violet isomer has already taken place. Subtraction of the equilibrium spectrum (mostly due to [**7**]$^+$, vide infra) from the intial spectrum of the mixture yields a binomial pentet ($g = 2.039$, $a_{Mo} = 27$ G, $a_{4H} = 8$ G, THF, −80 °C) for [**5**]$^+$ (see Figure 2a), which is essentially identical with the EPR spectrum previously reported for [**1a**]$^+$ ($g = 2.039$, $a_{Mo} = 28$ G, $a_{4H} = 8.5$ G, acetone, −80 °C).[2] This comparison is consistent with our previous conclusion that the electron couples to the four terminal butadiene hydrogen nuclei and not to those of the allyl ligand.[2] The EPR spectrum of [**7**]$^+$, on the other hand, exhibits a sextet at $g = 2.034$ in the EPR spectrum, due to the coupling to five protons ($a_{5H} = 7$ G) (see Figure 2b). In view of the septet patternobserved for [**1b**]$^+$ and assigned to the coupling to the four terminal butadiene protons and two *syn* allyl protons,[2] the EPR data of [**7**]$^+$ are easily interpreted as deriving from the coupling to the four terminal butadiene protons and one *syn* allyl proton, because one *syn* position is occupied by the ethyl group. The EPR data are thus consistent with the NMR assignment of the *syn* structure for the allyl ligand in the precursor **5**. The

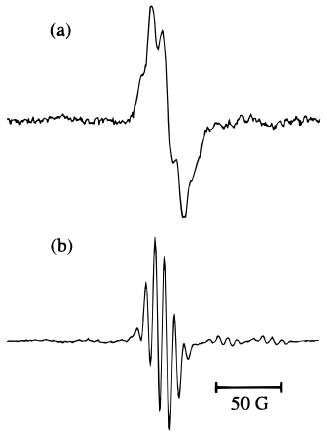

Figure 2. EPR spectra of [CpMo(1-*syn*-EtC_3H_4)(C_4H_6)]$^+$ in acetone: (a) the *prone*-allyl−*supine*-diene species ([**5**]$^+$), after subtraction of the spectrum of [**7**]$^+$, $T = -80$ °C; (b) the *supine*-allyl−*supine*-diene species ([**7**]$^+$), $T = -80$ °C.

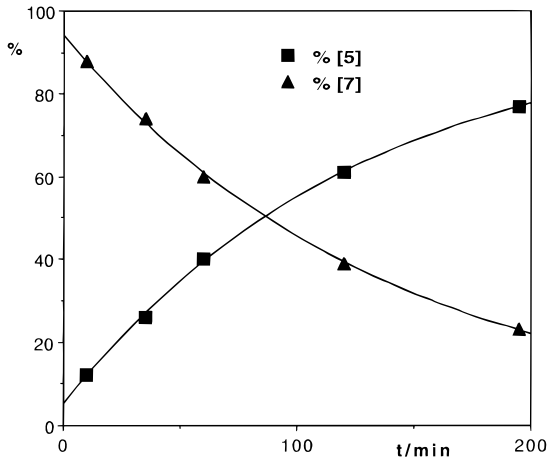

Figure 3. Kinetics of isomerization of **7** to **5** as determined by ^{1}H NMR integration (solvent C_6D_6, $T = 298$ K).

spectrum in Figure 2b does not exclude the presence of a small amount of [**5**]$^+$ at equilibrium.

Reduction of the 17-electron complex [**7**]$^+$ by cobaltocene gives the diamagnetic [CpMo(*syn-supine*-η-C_3H_4-1-Et)(*s-cis-supine*-η-C_4H_6)] (**7**), which quantitatively transforms to compound **5** as shown by the NMR monitoring. Again, this behavior parallels that reported for the allyl complex [**1b**]$^+$,[2] whose reduction afforded **1b** followed by the slow ($t_{1/2} = 6.5$ h) isomerization to the thermodynamically more stable **1a**. The kinetic analysis of the conversion of **7** to **5** (see Figure 3) yields the rate constant $k = 7.3 \times 10^{-3}$ min^{-1}, corresponding to a half-life of 95 min, and an extrapolated initial **7**:**5** ratio of 94.3:5.7. We assume that this also corresponds to the equilibrium ratio of [**7**]$^+$:[**5**]$^+$ before the cobaltocene reduction.

The cyclic voltammetric study of complexes **5** and [**7**]$^+$ are fully consistent with the results of the chemical investigation. At high sweep rates ($v > 0.2$ V s^{-1}) compound **5** exhibits an electrochemically reversible one-electron oxidation wave in THF at $E_{1/2} = -0.50$ V. However, at lower sweep rates the return reduction wave has a smaller intensity and is followed by a new reduction wave at $E_{1/2} = -0.86$ V (see Figure 4). The new wave is the follow-up of the fast chemical isomerization process from [**5**]$^+$ to [**7**]$^+$, as shown by the independent cyclic voltammetric study of isolated [**7**]$^+$.

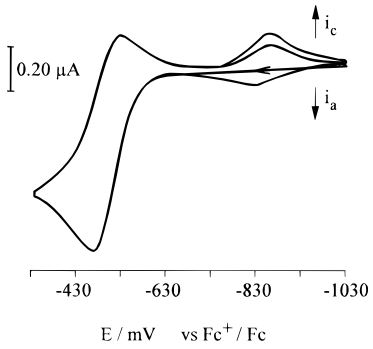

Figure 4. Cyclic voltammogram for compound **5** (10^{-3} M) (solvent THF, scan rate 10 mV s^{-1}).

Scheme 2

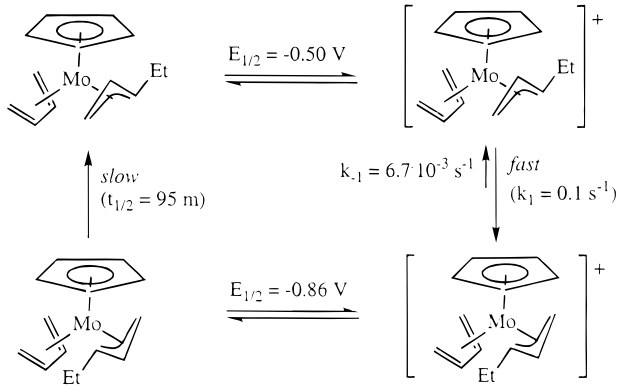

A decrease of the scan rate results in a decrease of the relative intensity for the cathodic wave corresponding to the conversion of $[\mathbf{5}]^+$ to **5**. This is as expected, because $[\mathbf{5}]^+$ has more time to isomerize to $[\mathbf{7}]^+$. In addition, there is a decrease in the relative intensity of the anodic wave that corresponds to the conversion of **7** to $[\mathbf{7}]^+$. Since we know from the independent NMR study (vide supra) that the isomerization of **7** to **5** is very slow and negligible within the time scale of the voltammetric experiment, the concentration reduction of **7** may only be attributed to a reversibility for the process interconverting $[\mathbf{5}]^+$ and $[\mathbf{7}]^+$ (see Scheme 2). A thin-layer CV study (see Figure 5) and subsequent simulation confirm this hypothesis and allow the determination of both forward and reverse isomerization rate constants ($k_1 = 0.1$ s^{-1}; $k_{-1} = 6.7 \times 10^{-3}$ s^{-1}). The equilibrium constant determined from these rates, $K = k_1/k_{-1} = 15$, corresponds to an equilibrium $[\mathbf{7}]^+$:$[\mathbf{5}]^+$ ratio of 93.8:6.2, in excellent agreement with the ratio suggested by the NMR study.

Protonation of Compound 5. In part 2 of this series,[3] we have shown that compound **1a** is electrophilically attacked by the proton at the terminal position of the allyl ligand, generating propene. Since the allyl ligand of the homologous compound **5** is asymmetric, it was of interest to probe the position of electrophilic attack for this compound. ^{1}H NMR monitoring shows the selective formation of *trans*-2-pentene. The absence of 1-pentene shows that the attack occurs regioselectively at the unsubstituted terminal allyl carbon, whereas the absence of *cis*-2-pentene further confirms the *syn* configuration of the coordinated allyl ligand.

Molecular Orbital Calculations. As the [CpMo(*s-cis-supine*-C_4H_6)(*s-trans*-C_4H_6)]$^+$ cation has not been crystallographically characterized, a tentative starting

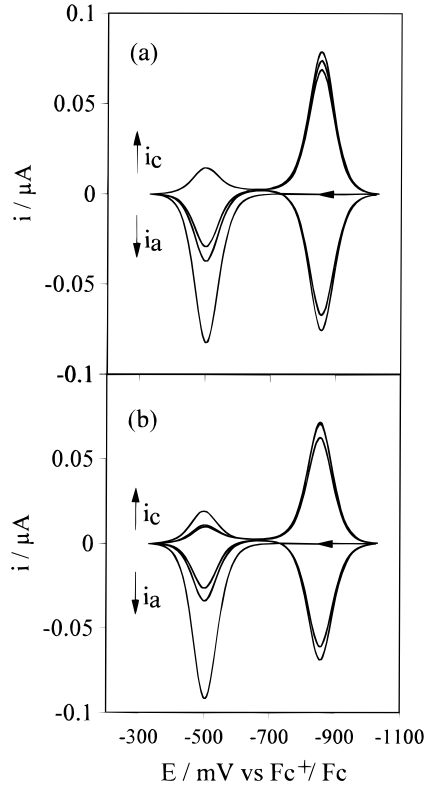

Figure 5. Thin-layer cyclic voltammograms for compound **5** (6×10^{-3} M) (solvent THF, scan rate 20 mV s^{-1}): (a) experimental; (b) simulated.

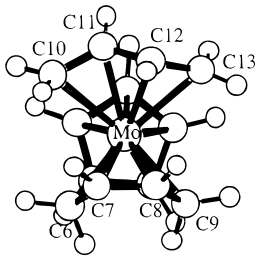

Figure 6. View of the B3LYP-optimized geometry of the [CpMo(*s-cis-supine*-C_4H_6)(*s-trans*-C_4H_6)]$^+$ cation, with the numbering scheme employed. The Cp carbon atoms are numbered C1−C5 (see Table 2).

geometry was constructed by combining the CpMo(*s-cis-supine*-C_4H_6) and CpMo(*s-trans*-C_4H_6) fragments from the X-ray-determined structures of **1a** and **1c**, respectively.[2] The geometry was subsequently optimized at the DFT-B3LYP level.[14] This computational method has proven quite reliable for both geometries and energies of transition metal complexes.[25,26] The optimized geometry, which differs only in minor details from the input geometry obtained from the X-ray-determined fragments, is shown in Figure 6. Selected bond distances are listed in Table 4.

The salient feature of the optimized structure (and the major difference relative to the tentative input geometry) is the lengthened distance between the metal and the *endo* terminal carbon of the *s-trans* ligand. The reason for this distortion is not obvious from the com-

(25) Musaev, D. G.; Froese, R. D. J.; Svensson, M.; Morokuma, K. *J. Am. Chem. Soc.* **1997**, *119*, 367−374.
(26) Musaev, D. G.; Svensson, M.; Morokuma, K.; Strömberg, S.; Zetterberg, K.; Siegbahn, P. E. M. *Organometallics* **1997**, *16*, 1933 and references therein.

Table 4. B3LYP-Optimized Distances (Å) for the [CpMo(*s-cis-supine*-C_4H_6)(*s-trans*-C_4H_6)]$^+$ Cation

Mo−Cp		Mo−(*s-cis*-C_4H_6)		Mo−(*s-trans*-C_4H_6)	
Mo−C1	2.436	Mo−C6	2.323	Mo−C10	2.426
Mo−C2	2.430	Mo−C7	2.408	Mo−C11	2.281
Mo−C3	2.384	Mo−C8	2.446	Mo−C12	2.377
Mo−C4	2.357	Mo−C9	2.374	Mo−C13	2.550
Mo−C5	2.372				
C1−C2	1.434	C6−C7	1.430	C10−C11	1.416
C2−C3	1.435	C7−C8	1.423	C11−C12	1.456
C3−C4	1.438	C8−C9	1.421	C12−C13	1.398
C4−C5	1.439				
C5−C1	1.446				

Table 5. Effective Atomic Charges for the [CpMo(*s-cis-supine*-C_4H_6)(*s-trans*-C_4H_6)]$^+$ Cation[a]

atom	B3LYP-Mulliken[b]	B3LYP−NBO[c]	FH-Mulliken[d]
Mo	−0.120	0.101	1.307
C1	0.114	0.081	0.011
C2	0.088	0.068	−0.006
C3	0.079	0.062	−0.020
C4	0.059	0.042	−0.037
C5	0.081	0.063	−0.027
C6	0.021	0.062	−0.135
C7	0.125	0.077	0.073
C8	0.175	0.103	0.024
C9	0.003	0.037	−0.114
C10	0.015	0.063	−0.089
C11	0.142	0.057	0.007
C12	0.169	0.058	0.040
C13	0.050	0.126	−0.032

[a] Atomic charges of the hydrogen atoms are summed into the attached carbon atom. [b] Mulliken population analysis of the B3LYP charge density matrix. [c] Natural population analysis of the B3LYP natural bond orbitals. [d] Mulliken population analysis of the Fenske−Hall molecular orbitals.

putational results. It is interesting to see, however, that the *endo* carbon atom corresponds to the position of nucleophilic attack. A naive idea for a rationalization of this distortion could involve the contribution of a diene−allyl resonance structure as shown in **II**. This

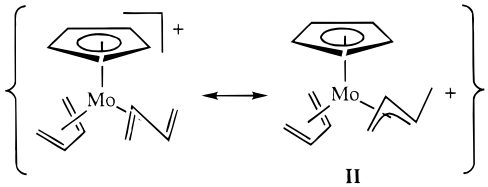

II

would rationalize the propensity of the terminal carbon toward attack by nucleophilic reagents, if this attack were charge-controlled. To probe for this effect, we have carried out an effective atomic charge analysis by three different methods: a Mulliken population analysis using the B3LYP density matrix, a natural population analysis of the B3LYP natural bond orbitals,[27] and a Mulliken population analysis of the molecular orbitals obtained from a Fenske−Hall calculation on the B3LYP-optimized geometry. The three results are compared in Table 5. The *s-trans endo* carbon (atom C13) indeed shows a more positive (or less negative) effective charge relative to the other diene terminal carbon atoms (C10, C9, and C6) at all levels of calculation. The charge

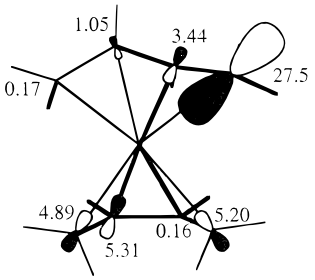

Figure 7. Qualitative view of the LUMO composition, limited to the two diene ligands, for [CpMo(*s-cis-supine*-C_4H_6)(*s-trans*-C_4H_6)]$^+$. Numbers represent the percent participation of atomic orbitals in the LUMO.

differences observed, however, are not large and indicate that a resonance form such as **II** is not very important.

A closer inspection of the optimized bond distances in Table 4, notably the shorter C12−C13 bond relative to the C10−C11 bond, reiterates the relative unimportance of the limiting form **II**. These data suggest rather, that the *s-trans* diene ligand is best considered as a diolefin with a loosely metal-bound C12−C13 ene function. The *s-cis* diene ligand, on the other hand, binds symmetrically to the metal center, in a way that is consistent with the classical Dewar−Chatt−Duncanson view of metal−diene bonding (donation from the π_2, back-bonding to the π_3 Huckel orbital).[28]

Anucleophilic attack at a π ligand is not likely to be charge-controlled but, rather, orbital-controlled. For this reason, an analysis of the LUMO was also carried out. From the Fenske−Hall results, the largest contribution to this orbital is from Mo atomic orbitals (36.7%). The second largest contribution is by far from the orbitals of the *endo* carbon of the *s-trans* butadiene ligand (27.5%, mostly p_z, the local *z* axis pointing toward the metal center). The relative contribution of the butadiene carbon orbitals to the LUMO is qualitatively illustrated in Figure 7. For an orbital-controlled nucleophilic addition, it is therefore expected that the nucleophile attacks the *endo* terminal carbon atom of the *s-trans* ligand, as experimentally observed. Attack at the metal center (the other large contributor with its atomic orbitals to the LUMO) rationalizes the path leading to the substitution products.

Discussion

Relative Reactivity of the Diene Ligands toward Nucleophiles. The reaction of [CpMo(*s-cis-supine*-C_4H_6)(*s-trans*-C_4H_6)]$^+$ (**2**) with nucleophilic reagents proceeds along two possible pathways, namely nucleophilic addition and substitution (see Scheme 3). The substitution pathway is preferred by neutral two-electron donors (MeCN and ^{t}BuNC), whereas the addition pathway is preferred by anionic reagents that can form stable allyl ligands. There are, however, exceptions to the above rule. The allyl Grignard reagent also affords minor amounts of the substitution product, while PMe_3 selectively affords the addition product. Numerous precedents for the nucleophilic addition of phosphorus nucleophiles to π ligands, both cyclic and acyclic, are available.[29] It does not seem, however, that the

(27) Reed, A. E.; Curtiss, L. A.; Weinhold, F. *Chem. Rev.* **1988**, *88*, 899−926.

(28) Yasuda, H.; Nakamura, A. *Angew. Chem., Int. Ed. Engl.* **1987**, *26*, 723−742.

(29) Kane-Maguire, L. A. P.; Honig, E. D.; Sweigart, D. A. *Chem. Rev.* **1984**, *84*, 525−543.

Scheme 3

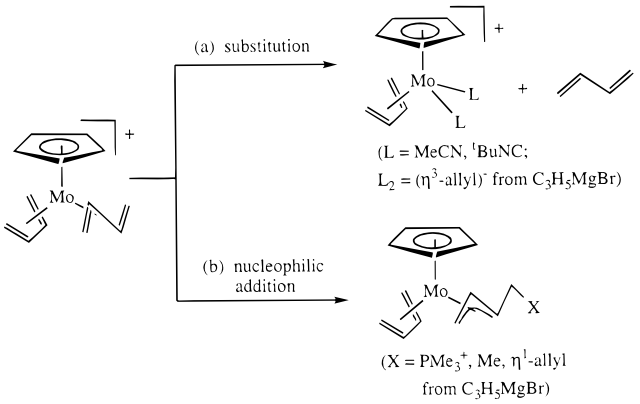

Scheme 4

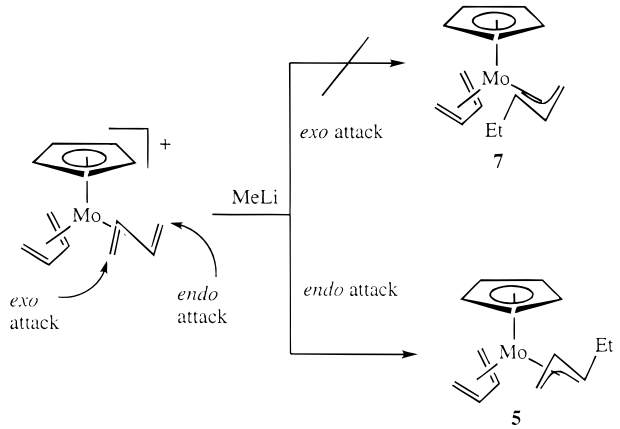

addition of a phosphorus nucleophile to a coordinated diene ligand (either *s-cis* or *s-trans*, cyclic or acyclic) has a precedent. All examples of additions to open π systems involve attack at a terminal position, e.g. at the pentadienyl ligand of $[Cp^*(\eta^5\text{-}C_5H_6\text{-}3\text{-}CH_3)Cr(CO)]^+$ to afford $[Cp^*(\eta^4\text{-}C_4H_4\text{-}2\text{-}CH_3\text{-}1\text{-}CH_2PMe_2Ph)Cr(CO)]^+$.[30]

Both reaction pathways observed for compound **2** involve the *s-trans* butadiene ligand, which is either replaced or subjected to nucleophilic addition. The *s-cis* ligand simply acts as a stabilizing spectator ligand like the cyclopentadienyl ring. Thus, the weaker binding of the *s-trans* diene ligand also corresponds to its stronger activation toward nucleophilic attack. As stated in the Introduction, nucleophilic additions to a coordinated *s-trans* diene have only been previously reported for $[CpMo(CO)_2(s\text{-}trans\text{-}CH_2{=}CHCH{=}CHR)]^+$ (R = H, Me).[11] The study of the $[CpMo(CO)_2(s\text{-}trans\text{-diene})]^+$ class is rendered difficult by the fast isomerization to the more stable *s-cis* isomer.[8] Compound **2**, on the other hand, is isomerically stable. Compounds of the isoelectronic CpMo(NO)(*s-trans*-diene) class are thermodynamically more stable than the *s-cis* isomers, but they are rather susceptible to electrophilic attack, e.g. by acetone[10] (cf. the reactivity toward protons of compounds **1**),[3] while the addition of nucleophilic reagents such as tertiary phosphines only leads with difficulty to products of addition to the metal center.[6] It is interesting to note that the *s-trans* diene ligand is also more susceptible than the *s-cis* conformer toward the electrophilic attack by protons (see Scheme 1), as shown by the comparative protonation study of compounds **1a**−**c**.[3]

Position of Nucleophilic Attack. In the nucleophilic addition reactions, the nucleophile attacks selectively the terminal *endo* position of the *s-trans* butadiene ligand. This is clearly shown by a rapid monitoring of the reaction with MeLi. Compound **5** is the only product formed instantaneously by the nucleophilic addition of MeLi to **2**. An attack at the *exo* position would yield compound **7** with a *supine* allyl ligand (Scheme 4). This alternative product was selectively obtained by another route (Scheme 2) and shown to convert into the isomer with the *prone* allyl ligand (compound **5**) slowly at room temperature ($t_{1/2}$ = 95 min). Thus, the formation of only **5** from this reaction proves the regioselective attack at the *endo* position of the *s-trans* diene ligand.

This experimental result is fully consistent with the idea of an orbital-controlled nucleophilic addition and with the computational results, which indicate a greater contribution of the *s-trans endo* carbon orbitals to the LUMO (see Figure 7). The computational results also rationalize the similar reactivity pathway reported for $[CpMo(CO)_2(s\text{-}trans\text{-}CH_2{=}CH{-}CH{=}CHMe)]^+$,[11] where the methyl group of the pentadiene ligand selectively occupies the *endo* position. This compound was shown to readily react with several nucleophiles, including H_2O, alcohols, amines, ethanethiol, and methyllithium. Small nucleophiles (H_2O, MeOH, EtOH, MeLi, and $Pr^i\text{-}NH_2$) gave only the sterically less favored *endo* addition product, whereas the largest nucleophile (Pr^i_2NH) gave predominantly the *exo* addition product. In our case, only the *endo* addition product was observed in all cases. It is clear that the *endo* carbon is the electronically preferred position for both substrates. The nature of the ancillary ligands (two CO ligands in place of *s-cis*-butadiene) may electronically affect the relative reactivity of the two lateral carbon atoms, or the relatively small size of the PMe_3 ligand and the absence of substituents on the *endo* carbon atom in **2** may be insufficient steric factors to divert the reactivity toward the *exo* position.

***supine/prone* Allyl Isomerism: Thermodynamic Preference and Interconversion Rates.** As stated above, it was possible to establish the regioselectivity of nucleophilic attack by virtue of the slow isomerization of the thermodynamically less favored *supine* allyl ligand in **7** to the more favored *prone* configuration in **5**. The situation encountered here parallels that of the parent compound **1** in its isomeric forms **1a** and **1b** (see Scheme 1).[2] The two systems differ only by the *syn*-ethyl substituent in the allyl ligand of **5**/**7**. While the *prone* allyl configuration in **1a** is thermodynamically preferred, the situation is reversed in the oxidized Mo(III) system, $[\mathbf{1b}]^+$ being favored over $[\mathbf{1a}]^+$. Another analogy between the two systems is the much faster rate of isomerization in the Mo(III) manifold (seconds at room temperature for $[\mathbf{5}]^+ \rightarrow [\mathbf{7}]^+$) than in the Mo(II) manifold ($t_{1/2}$ = 95 min at room temperature for **7** → **5**).

There are only small quantitative differences in the thermodynamic and kinetic parameters between the two systems. Compound **1** is obtained as an equilibrium 98:2 mixture of **1a** and **1b** at room temperature, which sets the relative free energy as 2.3 kcal/mol in favor of **1a**. The stability of $[\mathbf{1b}]^+$ relative to $[\mathbf{1a}]^+$ (ΔG = 5.8

(30) Shen, J. K.; Freeman, J. W.; Hallinan, N. C.; Rheingold, A. L.; Arif, A. M.; Ernst, R. D.; Basolo, F. *Organometallics* **1992**, *11*, 3215−3224.

Scheme 5

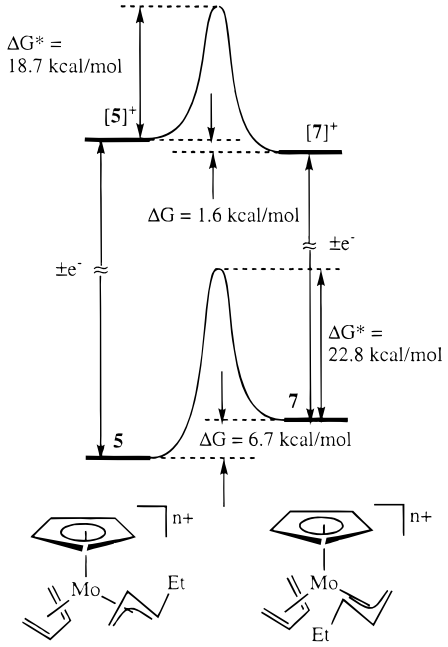

kcal/mol) was calculated from the relative stability of **1a**/**1b** and the difference in $E_{1/2}$ values for the two reversible redox processes (**1b** is oxidized at a potential 0.35 V more negative than **1a**).[2] By comparison, the NMR and CV simulation studies independently point to an equilibrium [**7**]$^+$/[**5**]$^+$ ratio of ca. 94:6 at room temperature, translating into a thermodynamic advantage of 1.6 kcal/mol for [**7**]$^+$ relative to [**5**]$^+$. The $E_{1/2}$ value for **7**/[**7**]$^+$ is 0.36 V more negative than the $E_{1/2}$ value for **5**/[**5**]$^+$ (both potentials being shifted negatively with respect to those of system **1**, as expected from the electron-releasing properties of the ethyl group). This sets a thermodynamic advantage of 6.7 kcal/mol for **5** relative to **7** (see Scheme 5). On the basis of this free energy difference, a Boltzmann ratio of 82 000:1 is calculated for **5**:**7**, justifying our inability to observe any amount of **7** at equilibrium by the ^{1}H NMR technique.

Concerning the rate of allyl isomerization, this is faster for the ethyl-bearing allyl complex relative to the parent allyl for both Mo(II) and Mo(III) systems. For the Mo(II) system, the isomerization half-life is 95 min for **7** compared with 6.5 h for **1b** under the same conditions, translating to a reduction in activation barrier of 0.8 kcal/mol (from 23.6 for **1b** to 22.8 kcal/mol for **7**). For the Mo(III) system, the rates determined by the electrochemical analysis set an activation barrier of 18.7 kcal/mol for the transformation of [**5**]$^+$ to [**7**]$^+$. Correspondingly, the activation barrier for the isomerization of [**1a**]$^+$ to [**1b**]$^+$ was previously estimated ca.

Scheme 6

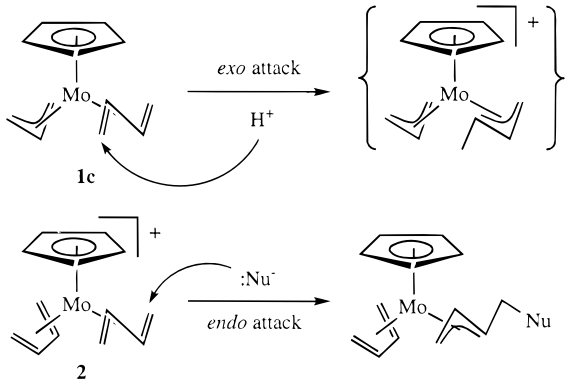

0.7 kcal/mol higher, at 19.4 kcal/mol.[2] Thus, the acceleration factor due to the introduction of a *syn*-Et substituent on the allyl ligand is approximately independent of the metal oxidation state.

Conclusions

The present study, in conjunction with the previous report in this series,[3] illustrates that the *s-trans* butadiene ligand in Cp-substituted Mo(II) complexes can be subjected to either electrophilic attack by protons (in the electron-rich neutral allyl derivative **1c**) or nucleophilic attack (in the electron-poorer, positively charged diene derivative **2**) (see Scheme 6). While the allyl ligand in **1c** competes with the *s-trans* diene ligand for the electrophilic reagent, the metal center competes for the nucleophilic reagent in **2**. In both cases, the *s-trans* diene ligand reacts preferentially relative to the *s-cis* diene. Finally, whereas the proton attack is presumably charge-controlled and takes place regioselectively at the diene *exo* position, the nucleophilic addition is orbital-controlled and takes place regioselectively at the diene *endo* position.

Acknowledgment. We are grateful to the NSF (Grant No. CHE-9508521) and to the Région Bourgogne for support of this work and Mrs. Raveau-Fouquet for technical assistance. The EPR upgrade was made possible in part by an NSF shared equipment (Grant No. CHE-9225064).

Supporting Information Available: Text giving a detailed description of experimental procedures and tables of crystal data and refinement parameters, fractional atomic coordinates, bond distances and angles, anisotropic thermal parameters, and hydrogen atom coordinates for the X-ray structure of compound **4** (9 pages). Ordering information is given on any current masthead page.